Zhenhua Xue, Wei Lin, Yang Chu, Wei Wei, Zhentian, Feng, and Junfeng Zhang, 2021, Late Triassic successive amalgamation between the South China and North China blocks: Insights from structural analysis and magnetic fabrics study of the Bikou Terrane and its adjacent area, northwestern Yangtze block, central China: GSA Bulletin, https://doi.org/10.1130/B36228.1.

Supplemental Material

Text. Basic principles of the anisotropy of magnetic susceptibility (AMS)

Figure S1. Photographs of supplementary shearing indicators of the structural kinematics.

Figure S2. Complete magnetic hysteresis data set for specimen selected from 34 sites.

Figure S3. Measurements of Isothermal Remanent Magnetization of specimen selected from 34 representative sites of the Bikou Terrane.

Figure S4. Thermo-magnetic experiments of specimen selected from 12 representative sites.

Figure S5. Mrs/Ms versus Hcr/Hc diagram from the selected specimen of the representative sites to define the size of magnetite.

Figure S6. Stereographic projection of the AMS directional fabrics and structural fabrics.

Basic principles of the anisotropy of magnetic susceptibility (AMS)

Put an object into an applied magnetic field (H), an induced magnitude (M) would be stimulated. The ratio of the induced and applied magnetic field is magnetic susceptibility (Borradaile and Henry, 1997; Borradaile and Jackson, 2004):

$$K_m = M/H$$

The Km is generally anisotropic, and the Km anisotropy is displayed by a magnetic susceptibility ellipsoid with three mutually orthogonal principal axes ($K_1 \geq K_2 \geq K_3$) (Tarling and Hrouda, 1993; Borradaile and Jackson, 2004). K_1 is referred to as the magnetic lineation representing the direction of the strongest induced magnetic field, and K_3 represents the pole to the magnetic foliation that delineates the weakest induced magnetic field. Bulk magnetic susceptibility within a sample is calculated as $(K_1 + K_2 + K_3)/3$ (Jelinek, 1981).

The Km is controlled by three types of magnetic carriers that contribute differently to the bulk magnetic susceptibility, including the paramagnetic, ferromagnetic, and diamagnetic carriers. Both the paramagnetic (e.g., phyllosilicates) and ferromagnetic (e.g., magnetite) carriers show an induced magnetic field of the same polarity as the external one, and the latter exhibits much higher susceptibility. The diamagnetic carrier (e.g., quartz and calcite) displays low intensity induced magnetic field of opposite polarity compared to the external field. Abundance, shape preferred orientation, distribution, etc., of all magnetic carriers in an object, determine the bulk Km and AMS fabrics (Borradaile and Jackson, 2004). Grain size and grain magnetostatic interaction of the ferromagnetic carrier determines the number of the magnetic domains (magnetic domain is a zone displaying a single magnetic pole) that also influence the induced

magnetic field (Tarling and Hrouda, 1993). According to grain size, the ferromagnetic carrier can be further classified as single domain (SD), multi-domain (MD), and pseudo-single domain (PSD) (Tarling and Hrouda, 1993). The MD and PSD carriers show a comparable AMS fabric with its grain shape, whereas the SD carrier shows an opposite AMS fabric comparing to its grain shape (Ferré et al., 2014).

Although the bulk Km is the sum effect of all magnetic carriers, the Km and magnetic fabrics are determined by the predominant carriers (Borradaile and Jackson, 2004). Even though tiny ferromagnetic carriers could result in high Km, they are generally distributed comparable with the aligned paramagnetic carriers (e.g., phyllosilicates), both of which display similar magnetic foliation and lineation (Borradaile and Henry, 1997; Borradaile and Jackson, 2010). After a careful recognition of the magnetic carriers, the magnetic foliations and lineations therefore could be applied to reveal mineral fabrics, and further to define the dominant foliations (= anisotropic plane) and mineral and stretching lineations (Borradaile and Henry, 1997; Borradaile and Jackson, 2004; Caricchi et al., 2016; Xue et al., 2017).

The corrected Pj value describes the eccentricity of the magnetic ellipsoid from a sphere (Pj = 1) to an ellipsoid (Pj>1)(Jelinek, 1981):

$$Pj = \exp\sqrt{2\sum(\ln K_i - \ln K_m)^2}$$

K_i refers to the three magnetic axes of K_1, K_2, and K_3. The shape parameter T value defines the shape of the magnetic ellipsoid ranging from prolate (T = –1) through neutral (T = 0) to oblate (T = +1) (Jelinek, 1981):

$$T = \frac{\ln(F)-\ln(L)}{\ln(F)+\ln(L)} \text{ where } L = \frac{K_1}{K_2} \text{ and } F = \frac{K_2}{K_3}$$

Correlations also exist between the Pj value and finite strain intensity and between the T value and strain ellipsoid geometry (Parés and van der Pluijm, 2002; Parsons et al., 2016; Marcén et al., 2018). Shape parameters of Pj and T values therefore (demonstrated by P_j and T values) can be used to reveal strain characteristics if the characteristics of the magnetic contributors are determined (Tarling and Hrouda, 1993; Borradaile and Henry, 1997; Parés and van der Pluijm, 2002).

REFERENCES CITED

Borradaile, G., and Henry, B., 1997, Tectonic applications of magnetic susceptibility and its anisotropy: Earth-Science Reviews, v. 42, no. 1, p. 49–93, https://doi.org/10.1016/S0012-8252(96)00044-X.

Borradaile, G.J., and Jackson, M., 2004, Anisotropy of magnetic susceptibility (AMS): magnetic petrofabrics of deformed rocks: Geological Society of London, Special Publications, v. 238, no. 1, p. 299–360, https://doi.org/10.1144/GSL.SP.2004.238.01.18.

Borradaile, G.J., and Jackson, M., 2010, Structural geology, petrofabrics and magnetic fabrics (AMS, AARM, AIRM): Journal of Structural Geology, v. 32, no. 10, p. 1519–1551, https://doi.org/10.1016/j.jsg.2009.09.006.

Caricchi, C., Cifelli, F., Kissel, C., Sagnotti, L., and Mattei, M., 2016, Distinct magnetic fabric in weakly deformed sediments from extensional basins and fold-and-thrust structures in the

Northern Apennine orogenic belt (Italy): Tectonics, v. 35, no. 2, p. 238–256, https://doi.org/10.1002/2015TC003940.
Dunlop, D.J., 2002, Theory and application of the Day plot (Mrs/Ms versus Hcr/Hc) 1. Theoretical curves and tests using titanomagnetite data: Journal of Geophysical Research. Solid Earth, v. 107, no. B3, p. EPM 4-1–EPM 4-22, https://www.doi.org/10.1029/2001JB000487.
Ferré, E.C., Gébelin, A., Till, J.L., Sassier, C., and Burmeister, K.C., 2014, Deformation and magnetic fabrics in ductile shear zones: A review: Tectonophysics, v. 629, p. 179–188, https://doi.org/10.1016/j.tecto.2014.04.008.
Jelinek, V., 1981, Characterization of the magnetic fabric of rocks: Tectonophysics, v. 79, no. 3–4, p. T63–T67, https://doi.org/10.1016/0040-1951(81)90110-4.
Marcén, M., Casas-Sainz, A.M., Román-Berdiel, T., Oliva-Urcia, B., Soto, R., and Aldega, L., 2018, Kinematics and strain distribution in an orogen-scale shear zone: Insights from structural analyses and magnetic fabrics in the Gavarnie thrust, Pyrenees: Journal of Structural Geology, v. 117, p. 105–123, https://doi.org/10.1016/j.jsg.2018.09.008.
Parés, J.M., and van der Pluijm, B.A., 2002, Evaluating magnetic lineations (AMS) in deformed rocks: Tectonophysics, v. 350, no. 4, p. 283–298, https://doi.org/10.1016/S0040-1951(02)00119-1.
Parsons, A.J., Ferré, E.C., Law, R.D., Lloyd, G.E., Phillips, R.J., and Searle, M.P., 2016, Orogen-parallel deformation of the Himalayan midcrust: Insights from structural and magnetic fabric analyses of the Greater Himalayan Sequence, Annapurna-Dhaulagiri Himalaya, central Nepal: Tectonics, v. 35, no. 11, p. 2515–2537, https://doi.org/10.1002/2016TC004244.
Tarling, D., and Hrouda, F., 1993, Magnetic anisotropy of rocks: Springer Science & Business Media.
Xue, Z., Martelet, G., Lin, W., Faure, M., Chen, Y., Wei, W., Li, S., and Wang, Q., 2017, Mesozoic crustal thickening of the Longmenshan belt (NE Tibet, China) by imbrication of basement slices: insights from structural analysis, petrofabric and magnetic fabric studies, and gravity modeling: Tectonics, p. 3110–3134, https://doi.org/10.1002/2017TC004754.

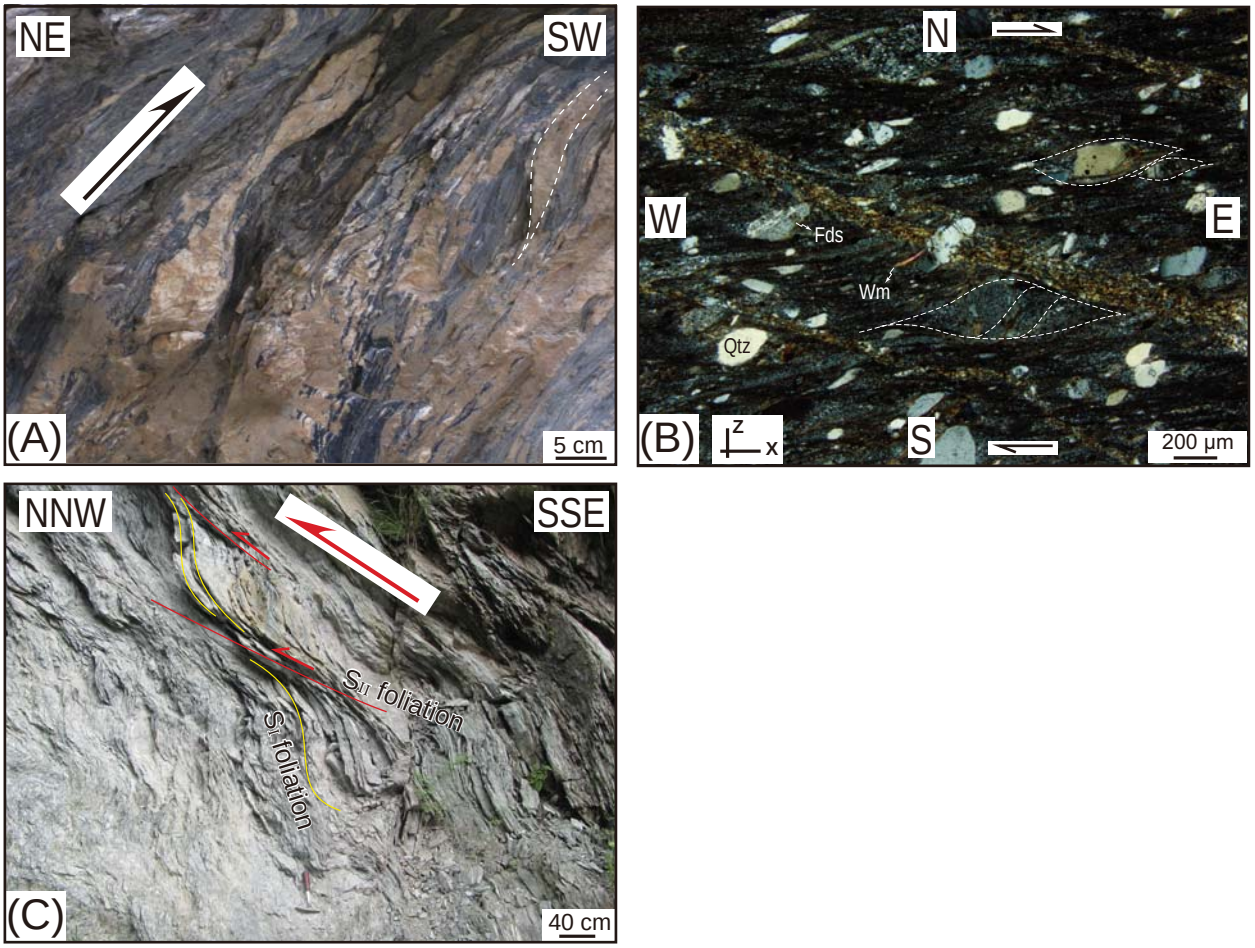

Figure S1. (A) Deflected intercalate thinly-bedded limestone and marl and sigmoid limestone lenses involved into the top-to-the-SW shearing [33°16.289'N, 105°11.339'E]. (B) Sigmoidal quartz and feldspar clasts and deflected white mica within mylonite in the northern Bikou Terrane, indicating a dextral sense of shear. CPL [33°08.442'N, 105°18.177'E]. (C) Late-stage S_{II} foliation cuts and displaces an early-stage foliation (possibly S_I), both of which form a shear band incorporating to the top-to-the-NNW thrusting.

Figure S1

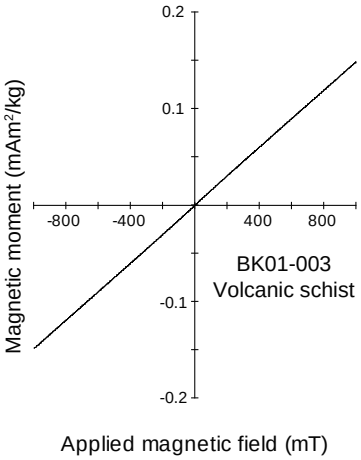
Magnetic moment (mAm²/kg)
0.2
0.1
-0.1
-0.2
-800
-400
400
800
BK01-003
Volcanic schist
Applied magnetic field (mT)

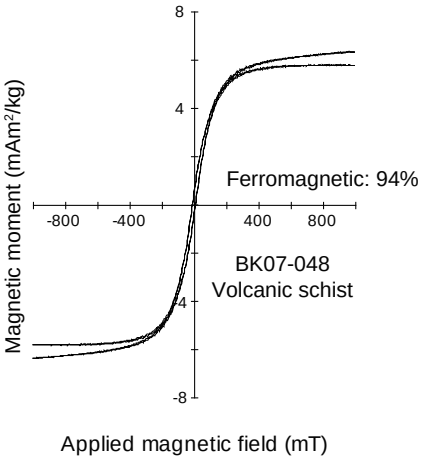
Magnetic moment (mAm²/kg)
8
4
-4
-8
-800
-400
400
800
Ferromagnetic: 94%
BK07-048
Volcanic schist
Applied magnetic field (mT)

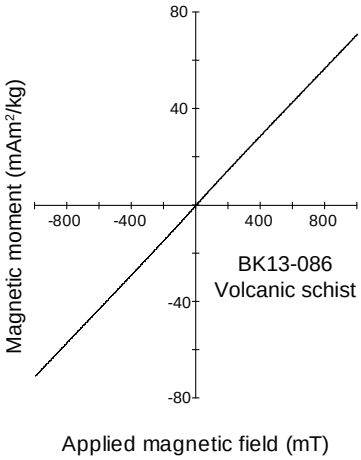
Magnetic moment (mAm²/kg)
80
40
-40
-80
-800
-400
400
800
BK13-086
Volcanic schist
Applied magnetic field (mT)

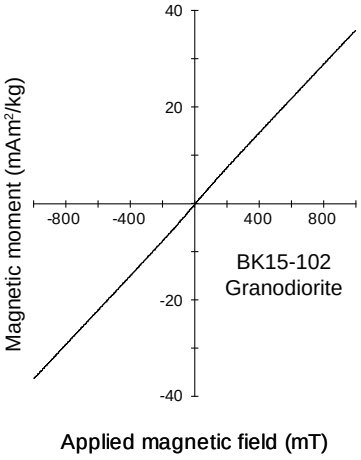
Magnetic moment (mAm²/kg)
40
20
-20
-40
-800
-400
400
800
BK15-102
Granodiorite
Applied magnetic field (mT)

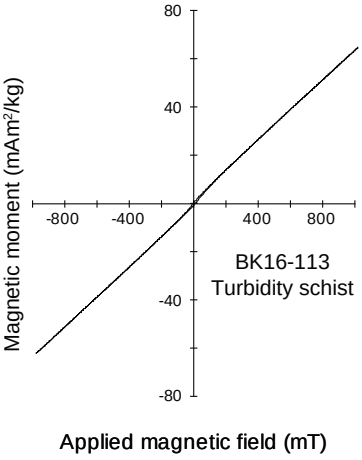
Magnetic moment (mAm²/kg)
80
40
-40
-80
-800
-400
400
800
BK16-113
Turbidity schist
Applied magnetic field (mT)

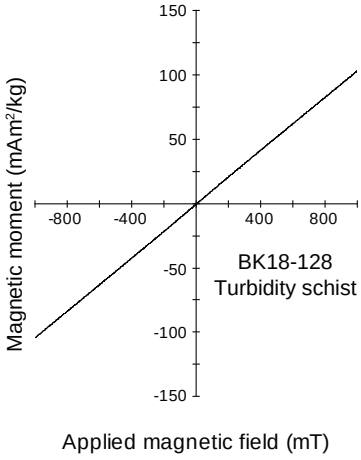
Magnetic moment (mAm²/kg)
150
100
50
-50
-100
-150
-800
-400
400
800
BK18-128
Turbidity schist
Applied magnetic field (mT)

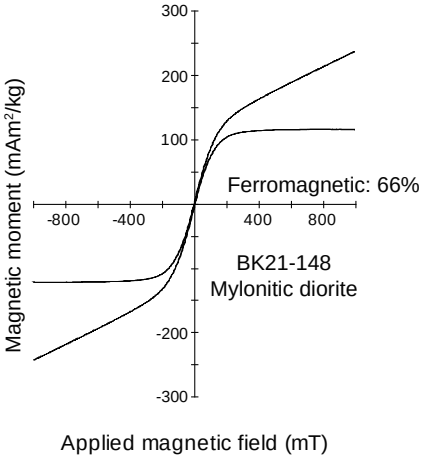
Magnetic moment (mAm²/kg)
300
200
100
-200
-300
-800
-400
400
800
Ferromagnetic: 66%
BK21-148
Mylonitic diorite
Applied magnetic field (mT)

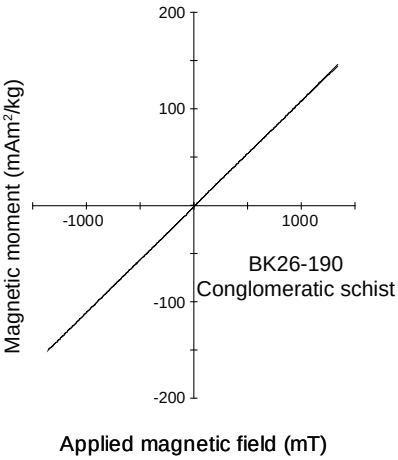
Magnetic moment (mAm²/kg)
200
100
-100
-200
-1000
1000
BK26-190
Conglomeratic schist
Applied magnetic field (mT)

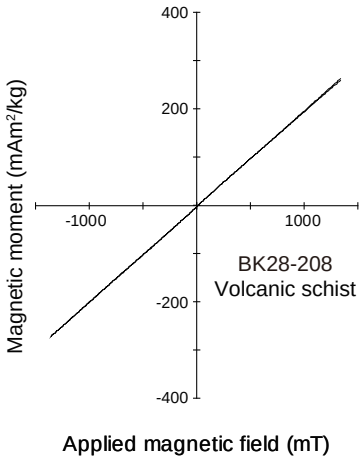
Magnetic moment (mAm²/kg)
400
200
-200
-400
-1000
1000
BK28-208
Volcanic schist
Applied magnetic field (mT)

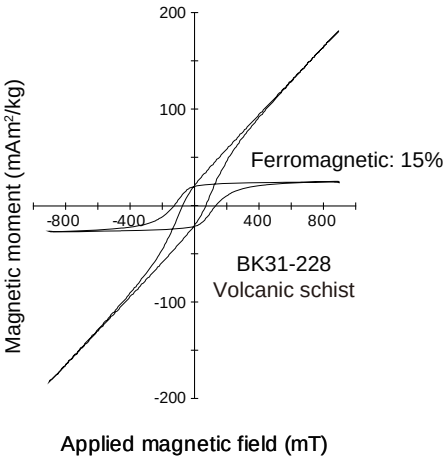
Magnetic moment (mAm²/kg)
200
100
-100
-200
-800
-400
400
800
Ferromagnetic: 15%
BK31-228
Volcanic schist
Applied magnetic field (mT)

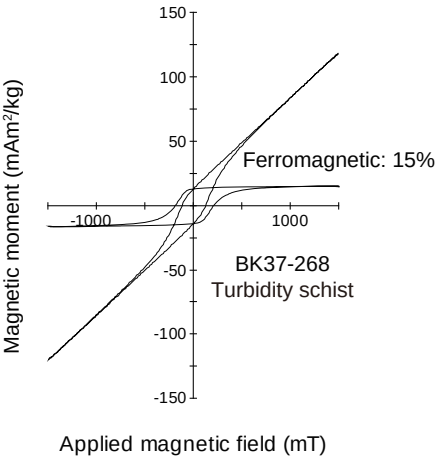
Magnetic moment (mAm²/kg)
150
100
50
-50
-100
-150
-1000
1000
Ferromagnetic: 15%
BK37-268
Turbidity schist
Applied magnetic field (mT)

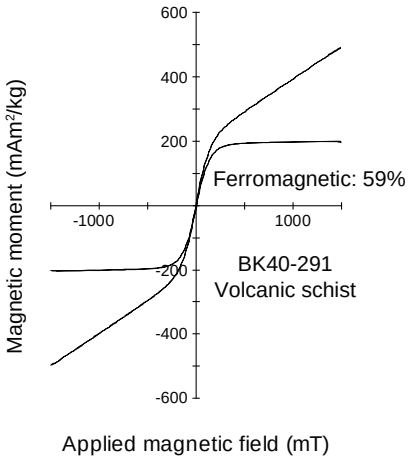
Magnetic moment (mAm²/kg)
600
400
200
-200
-400
-600
-1000
1000
Ferromagnetic: 59%
BK40-291
Volcanic schist
Applied magnetic field (mT)

Figure S1 continued

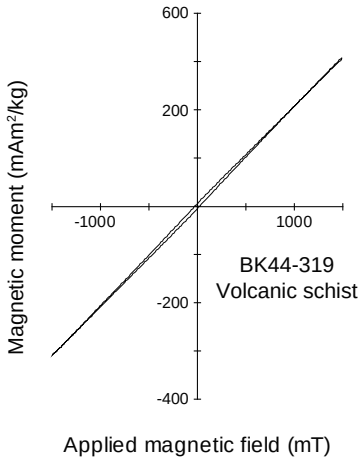

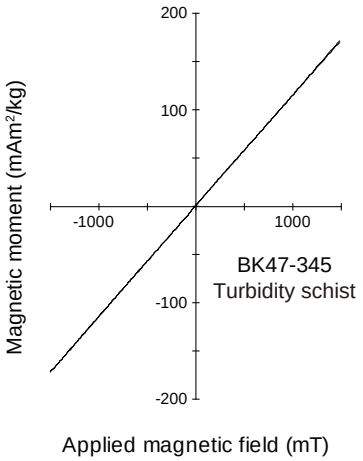

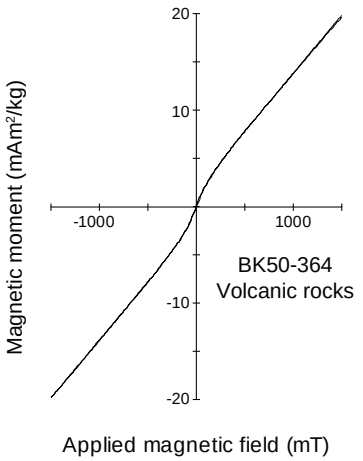

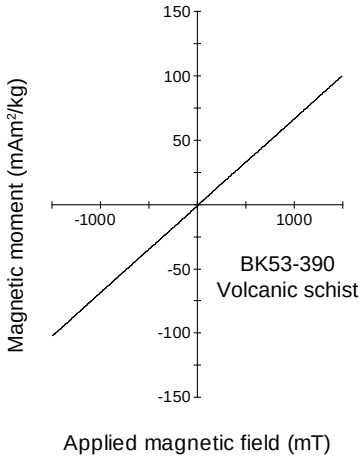

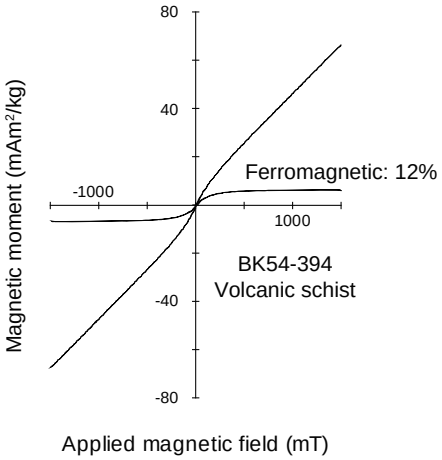

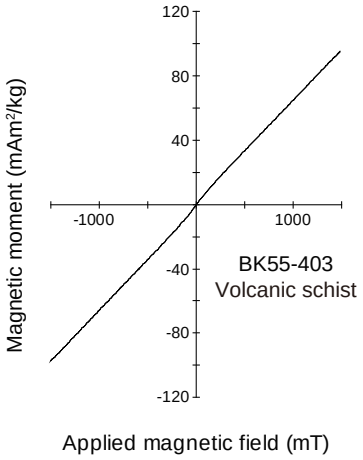

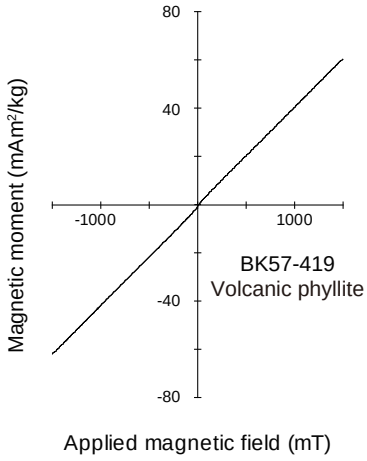

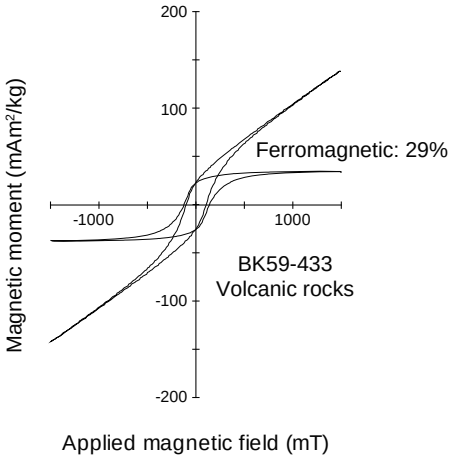

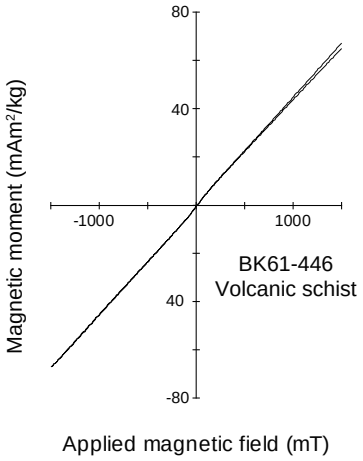

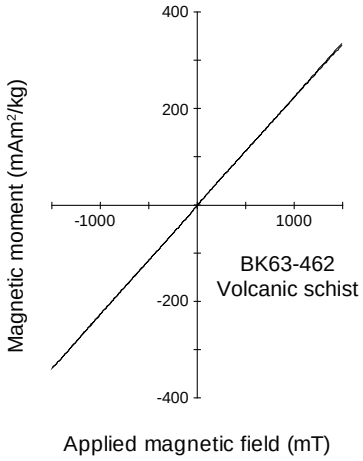

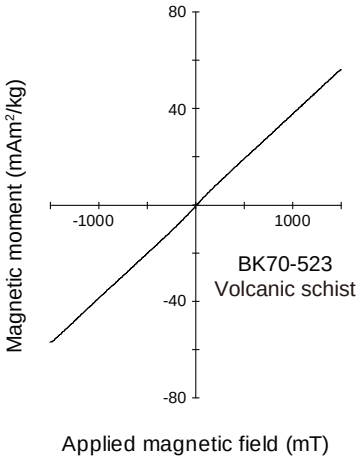

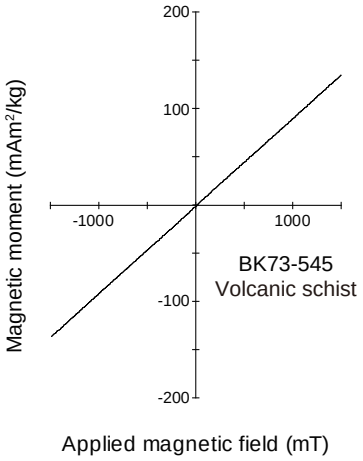

Figure S1 continued

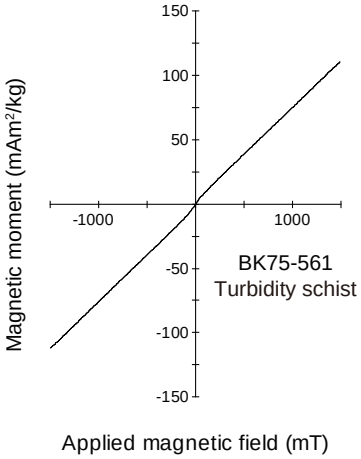

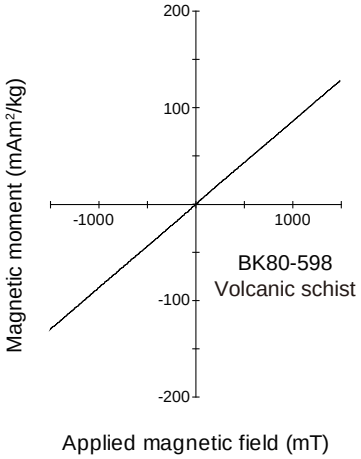

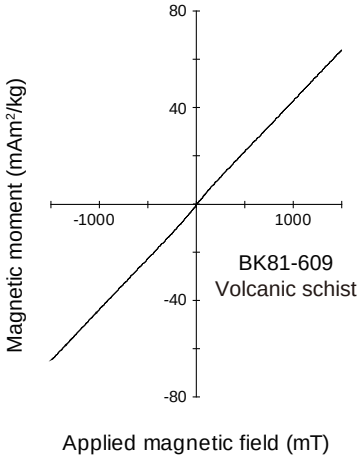

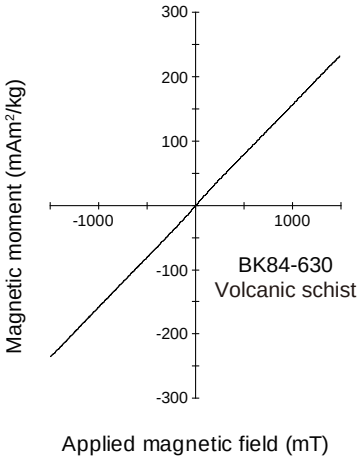

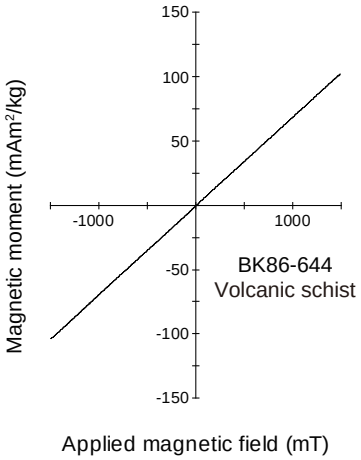

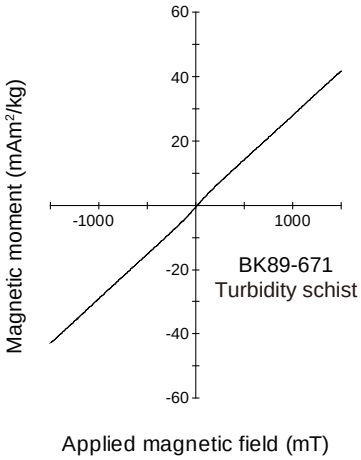

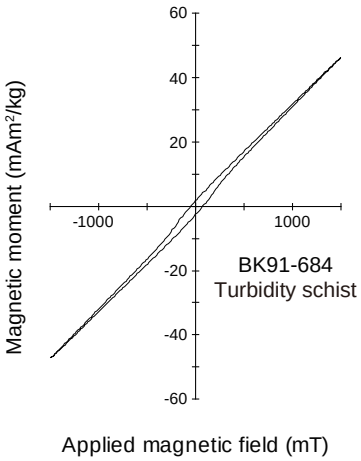

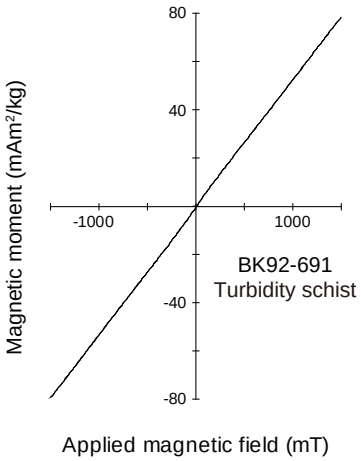

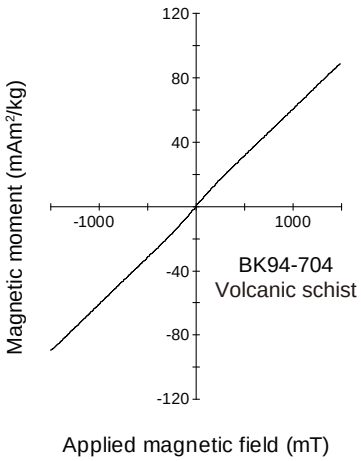

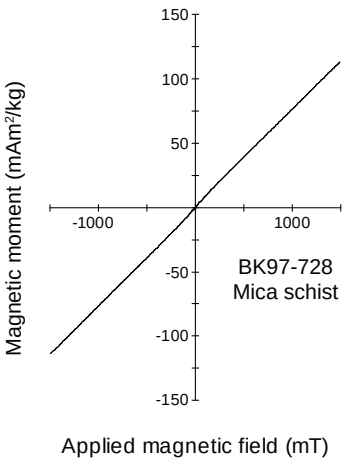

Figure S3. Measurements of Isothermal Remanent Magnetization of specimen selected from 34 representative sites of the Bikou Terrane.

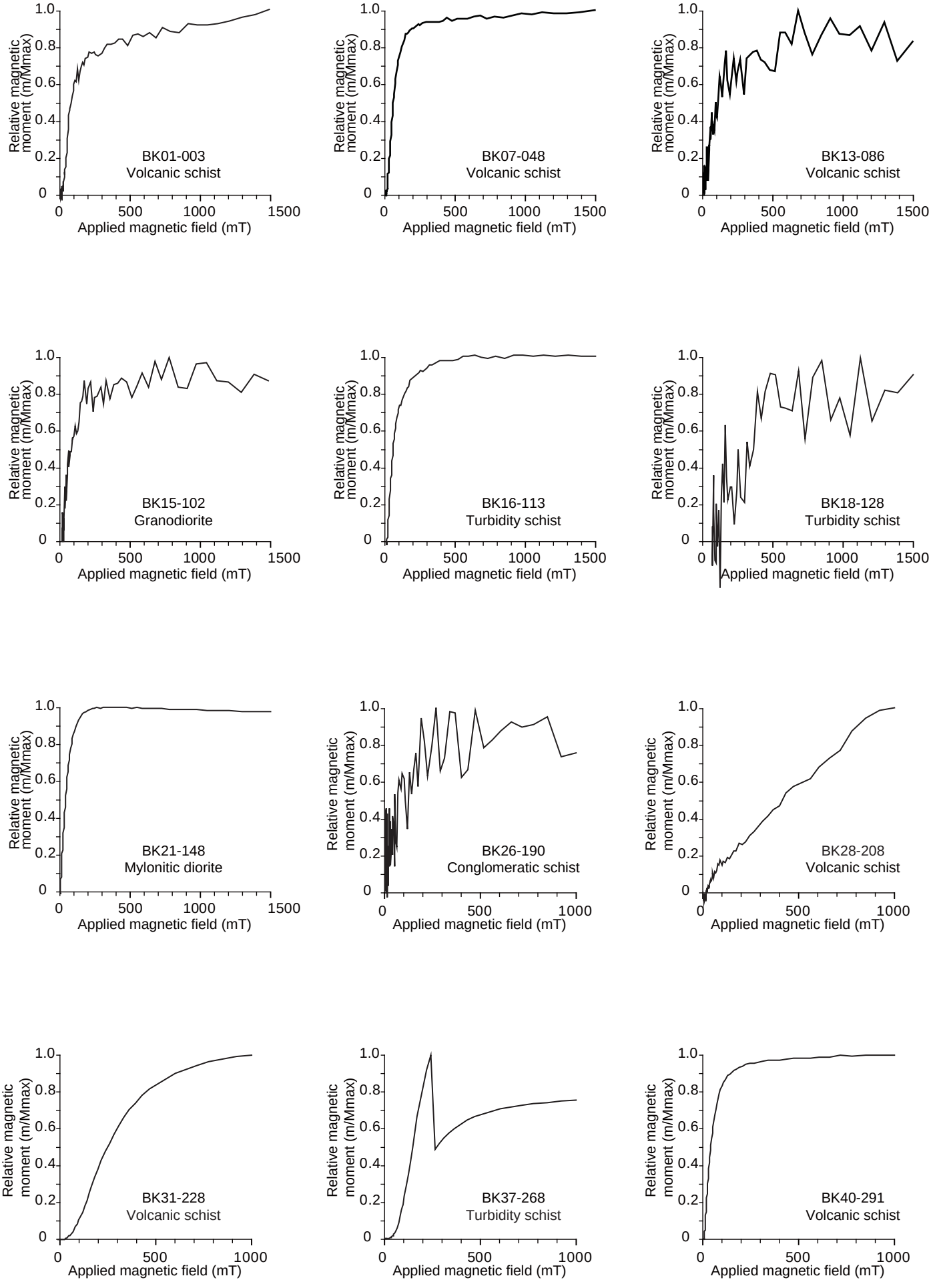

Figure S3 continued

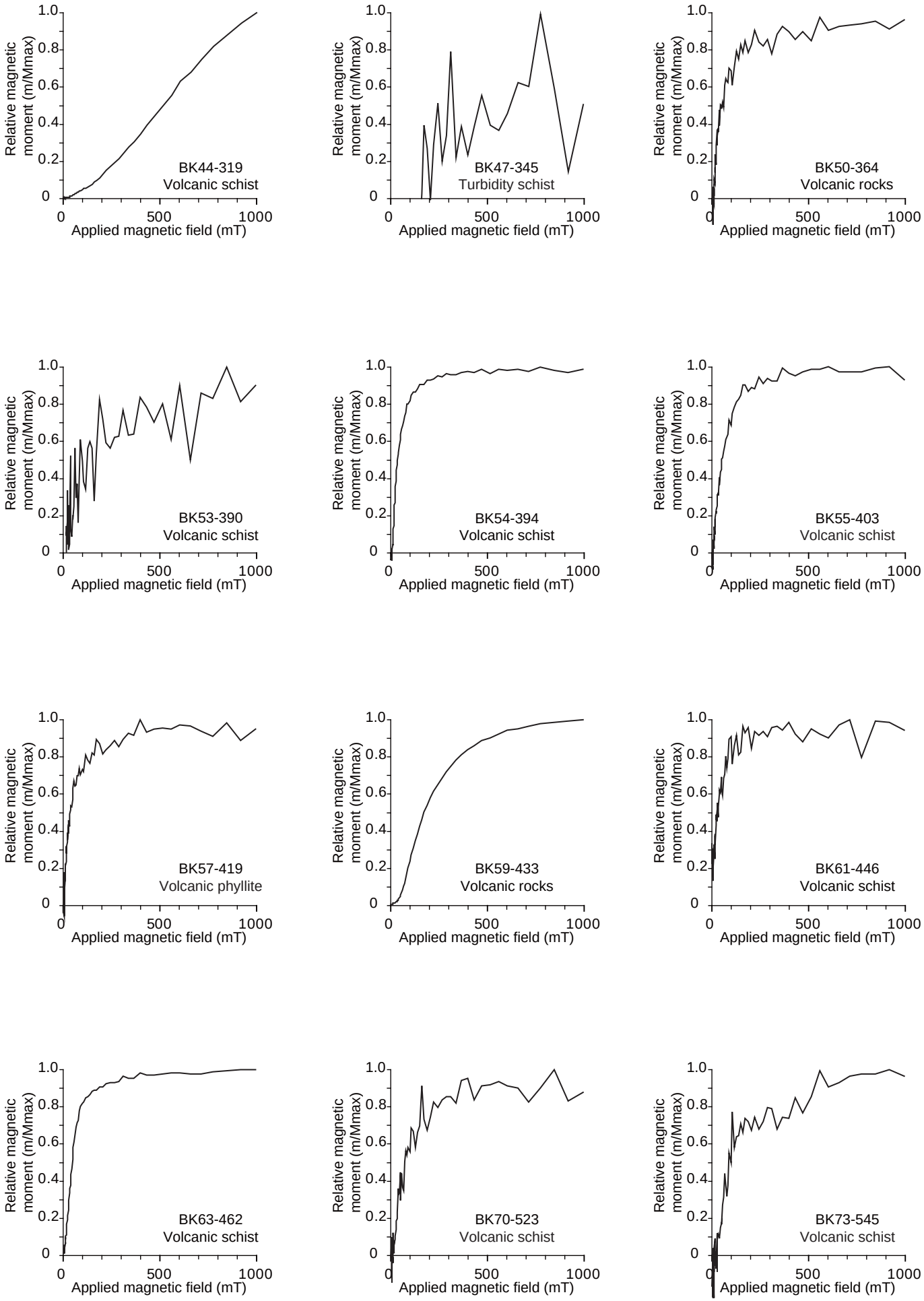

Figure S2 continued

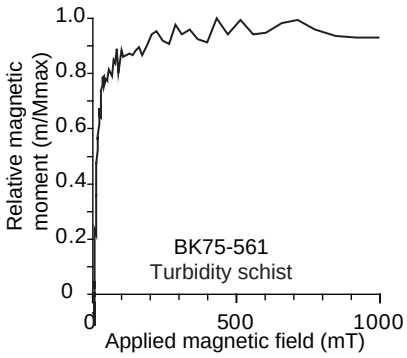

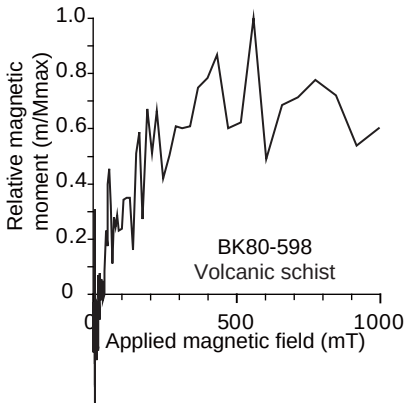

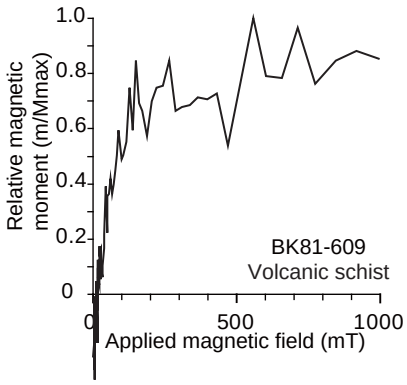

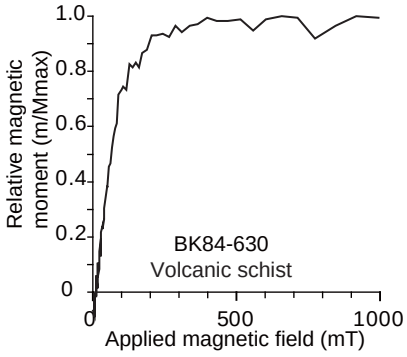

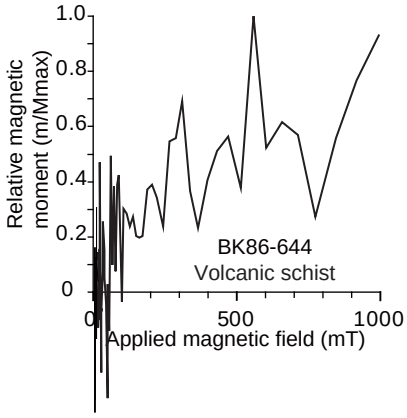

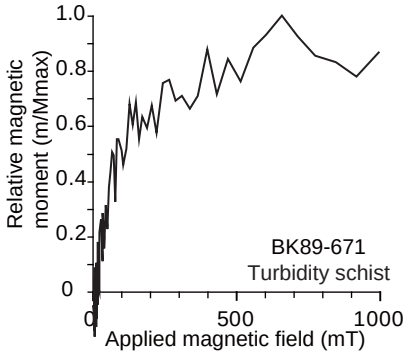

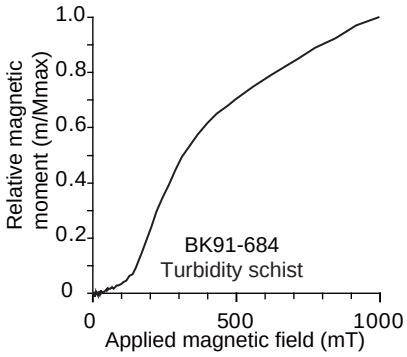

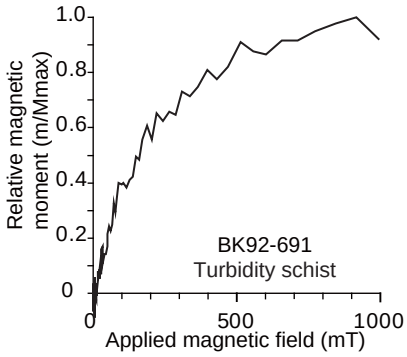

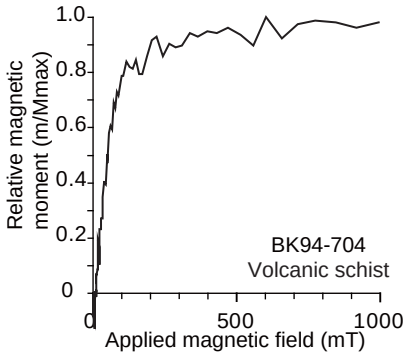

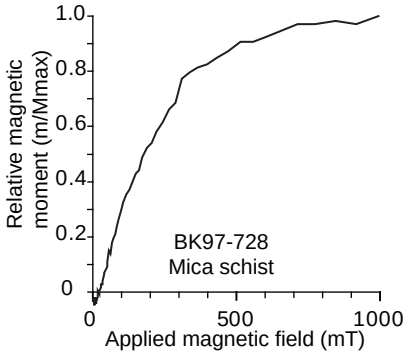

Figure S4. Thermo-magnetic experiments of specimen selected from 12 representative sites.

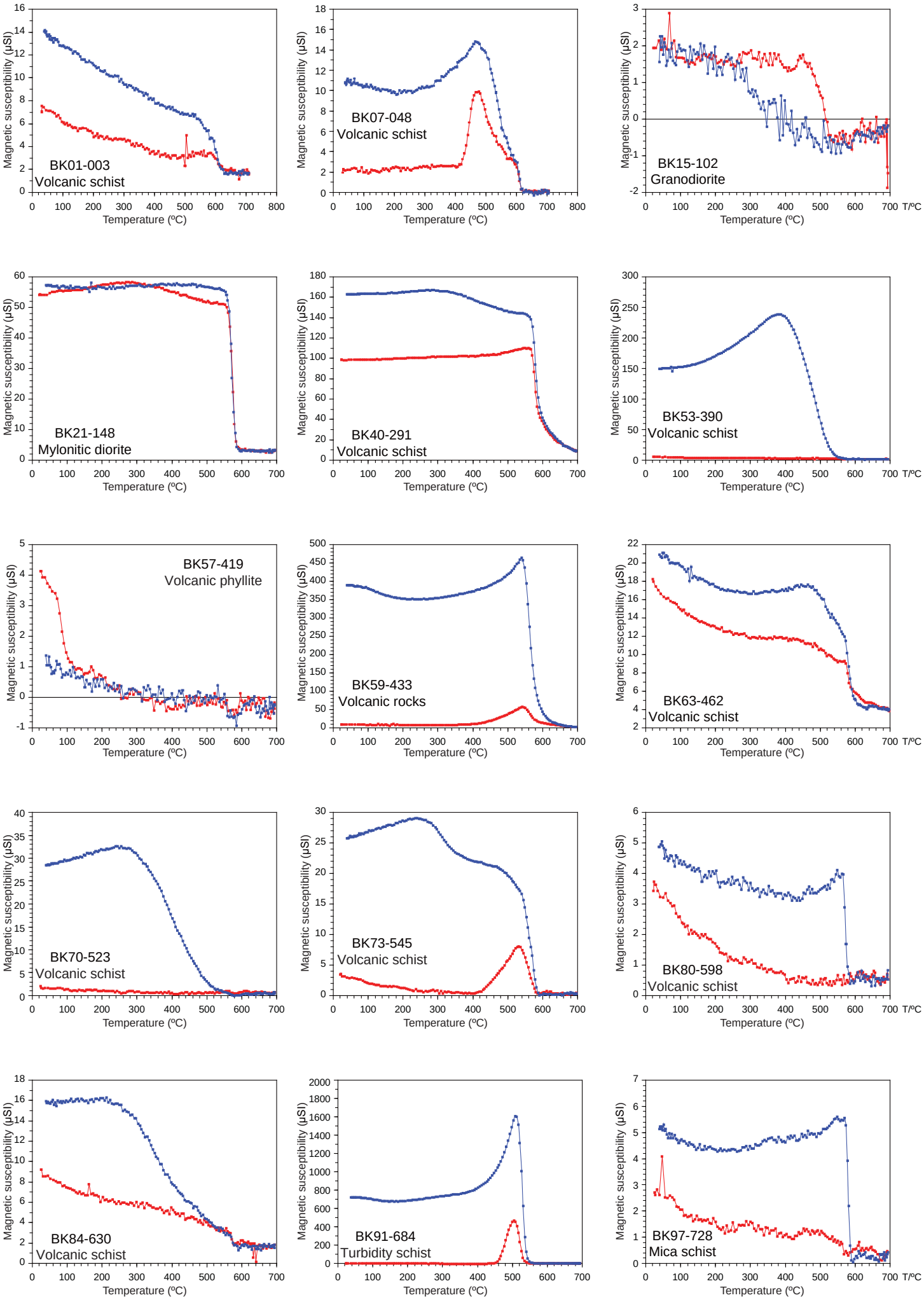

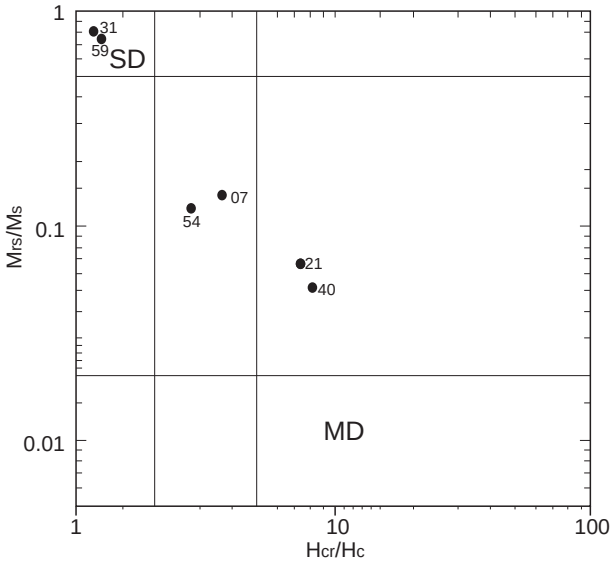

Figure S5. Mrs/Ms versus Hcr/Hc diagram from the selected specimen of the representative sites to define the size of magnetite. Mrs: remanence of saturation magnetization after removing the applied field, Ms: saturation magnetization under applied field, Hcr: coercivity of remanence after removing the applied field, Hc: coercivity under applied field, SD: single domain, PSD: pseudo single domain, and MD: multi-domain. Calculating methods are after Dunlop (2002).

Dunlop, D. J., 2002, Theory and application of the Day plot (Mrs/Ms versus Hcr/Hc) 1. Theoretical curves and tests using titanomagnetite data: Journal of Geophysical Research: Solid Earth, v. 107, no. B3, p. EPM 4-1-EPM 4-22, doi: 10.1029/2001JB000487.

Figure S6

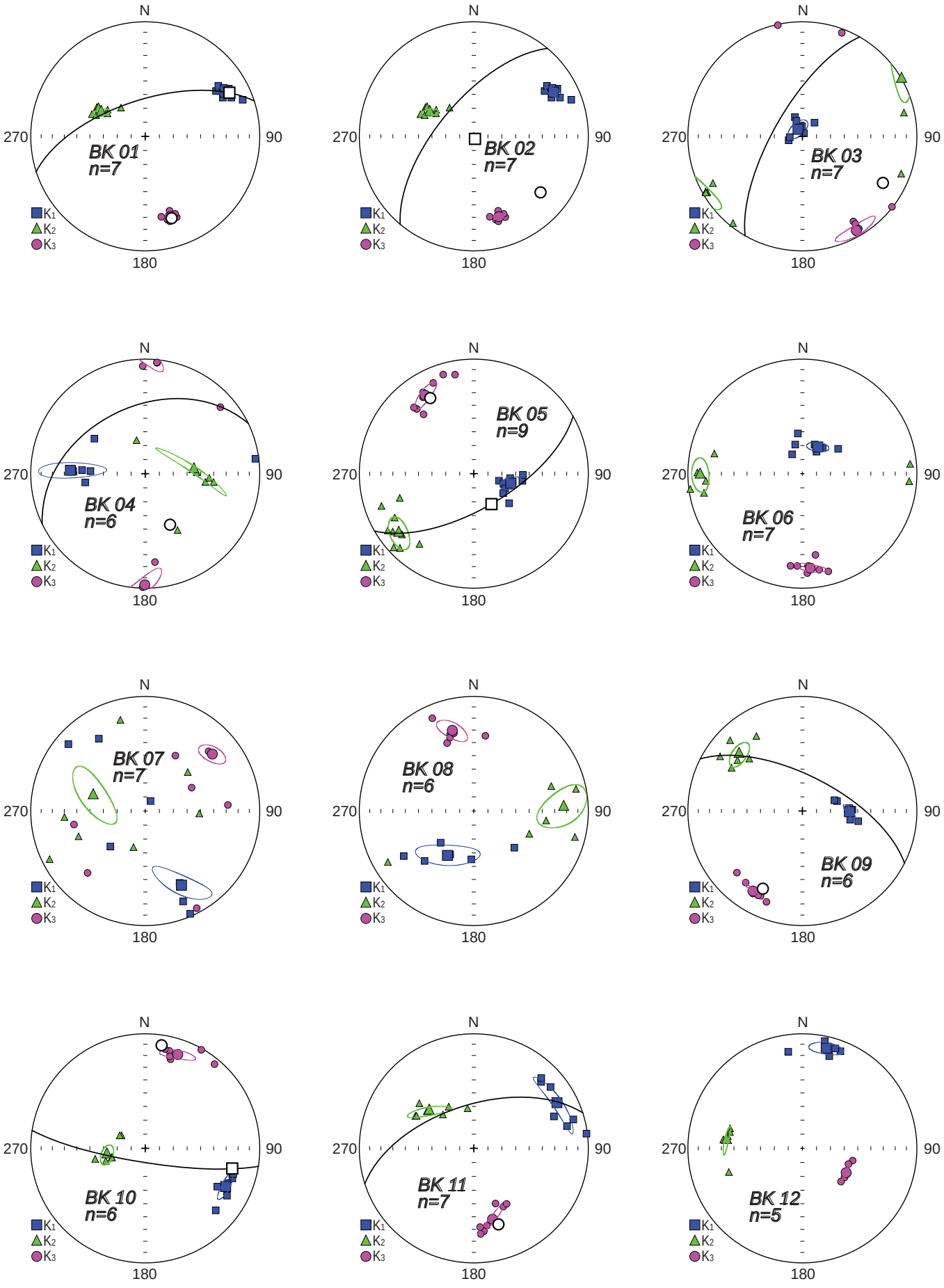
N
270
90
180
BK 01
n=7
BK 02
n=7
BK 03
n=7
BK 04
n=6
BK 05
n=9
BK 06
n=7
BK 07
n=7
BK 08
n=6
BK 09
n=6
BK 10
n=6
BK 11
n=7
BK 12
n=5
K1
K2
K3

Figure S6 continued

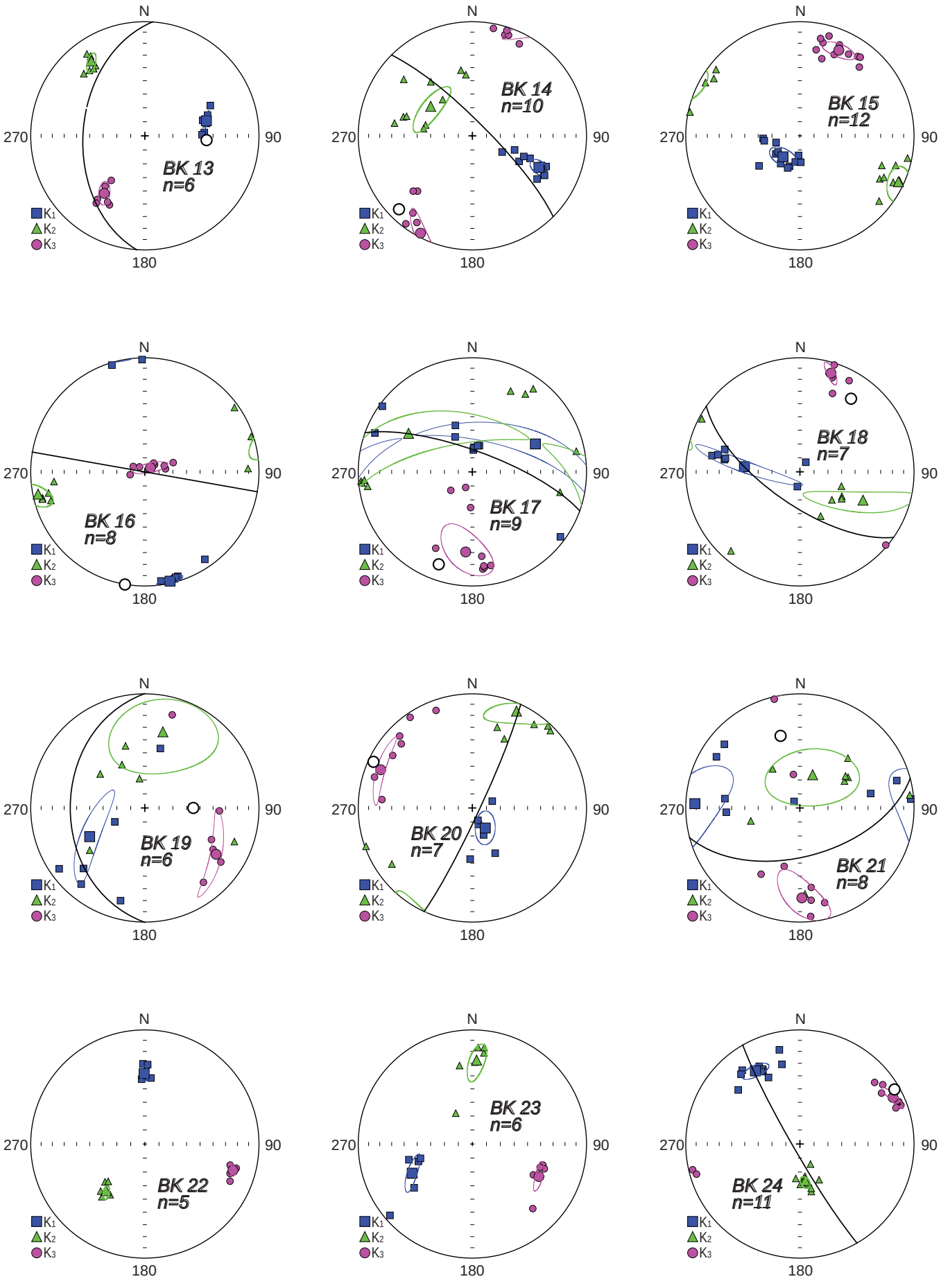

Figure S6 continued

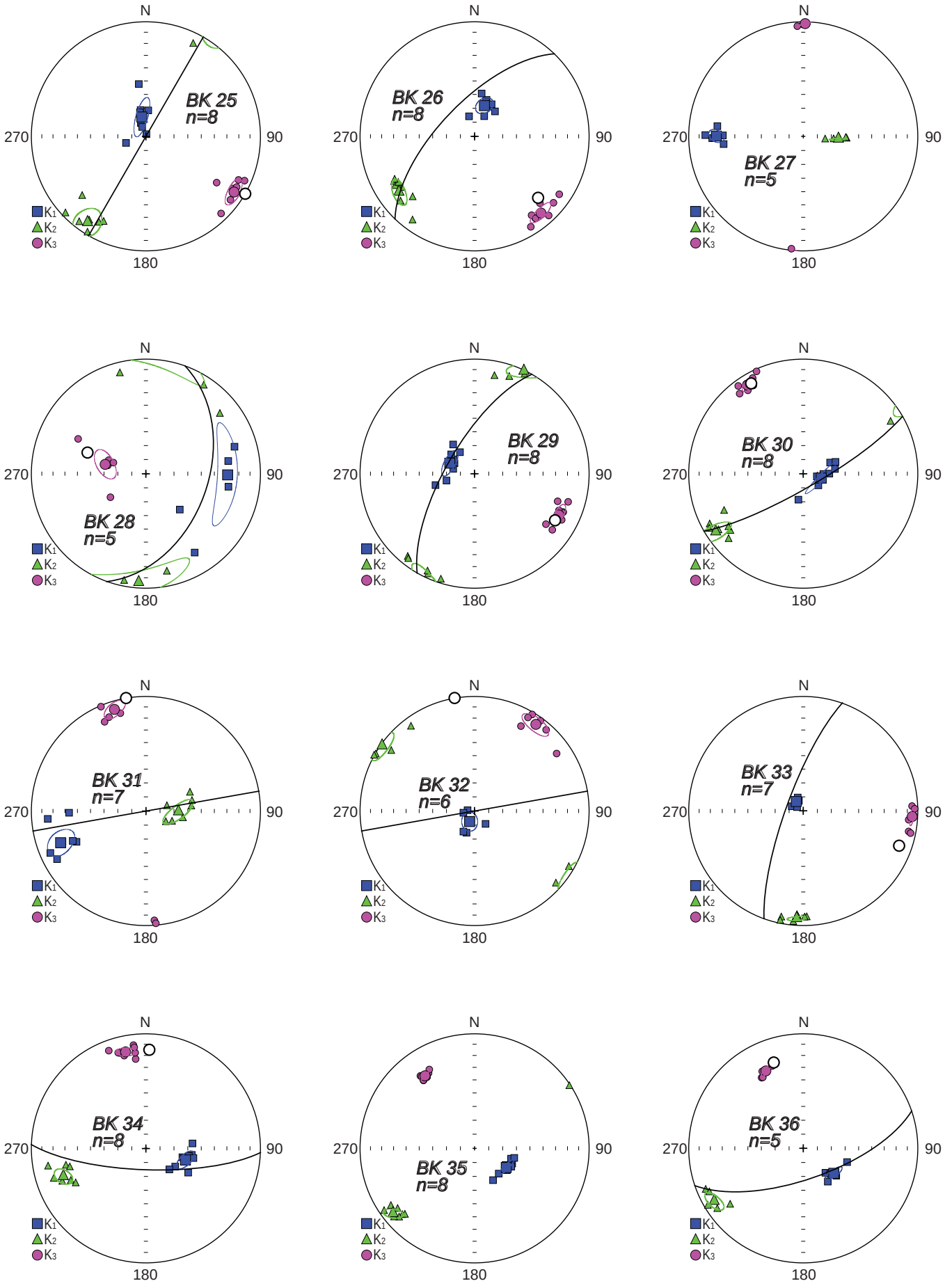

Figure S6 continued

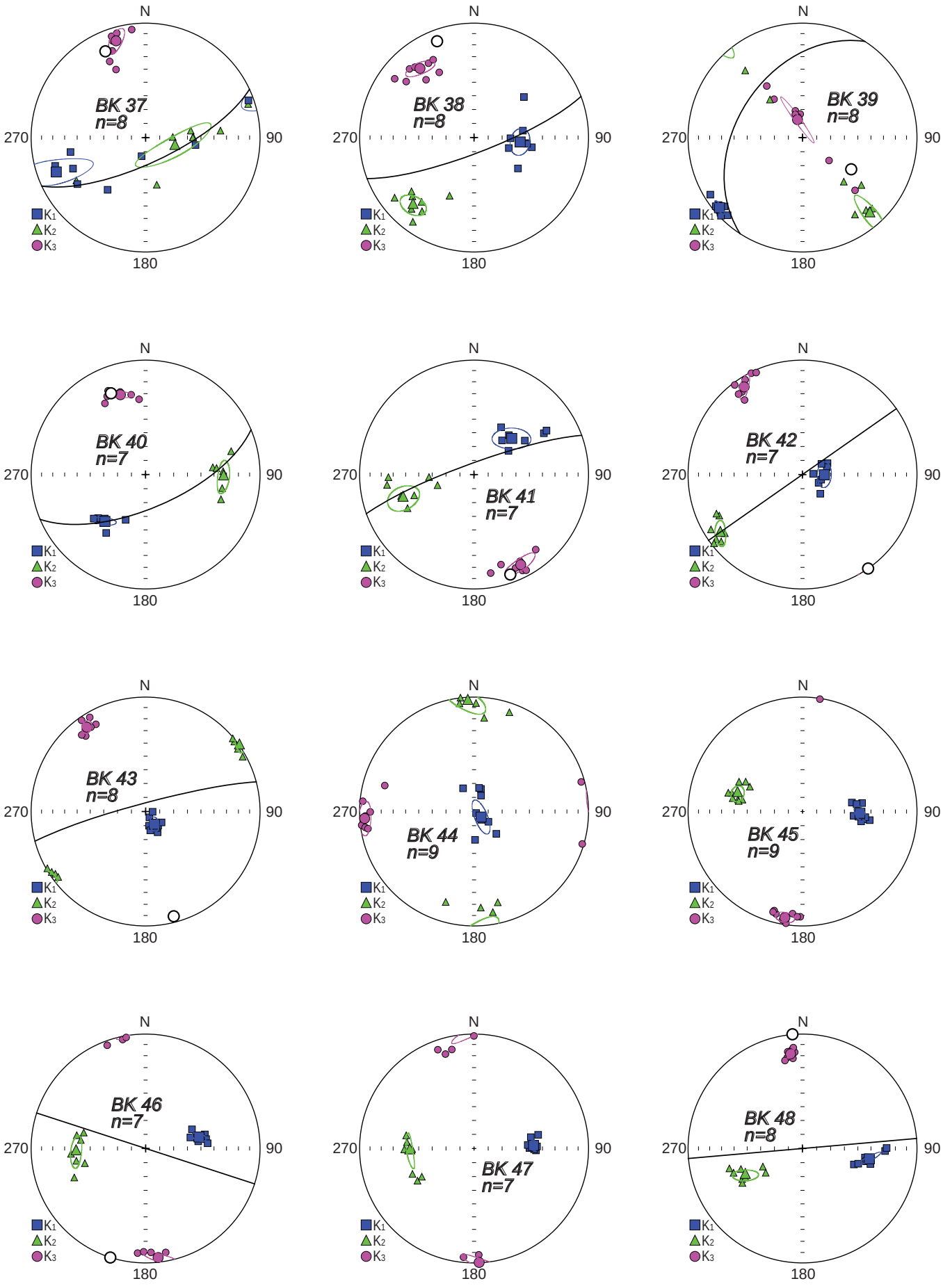

Figure S6 continued

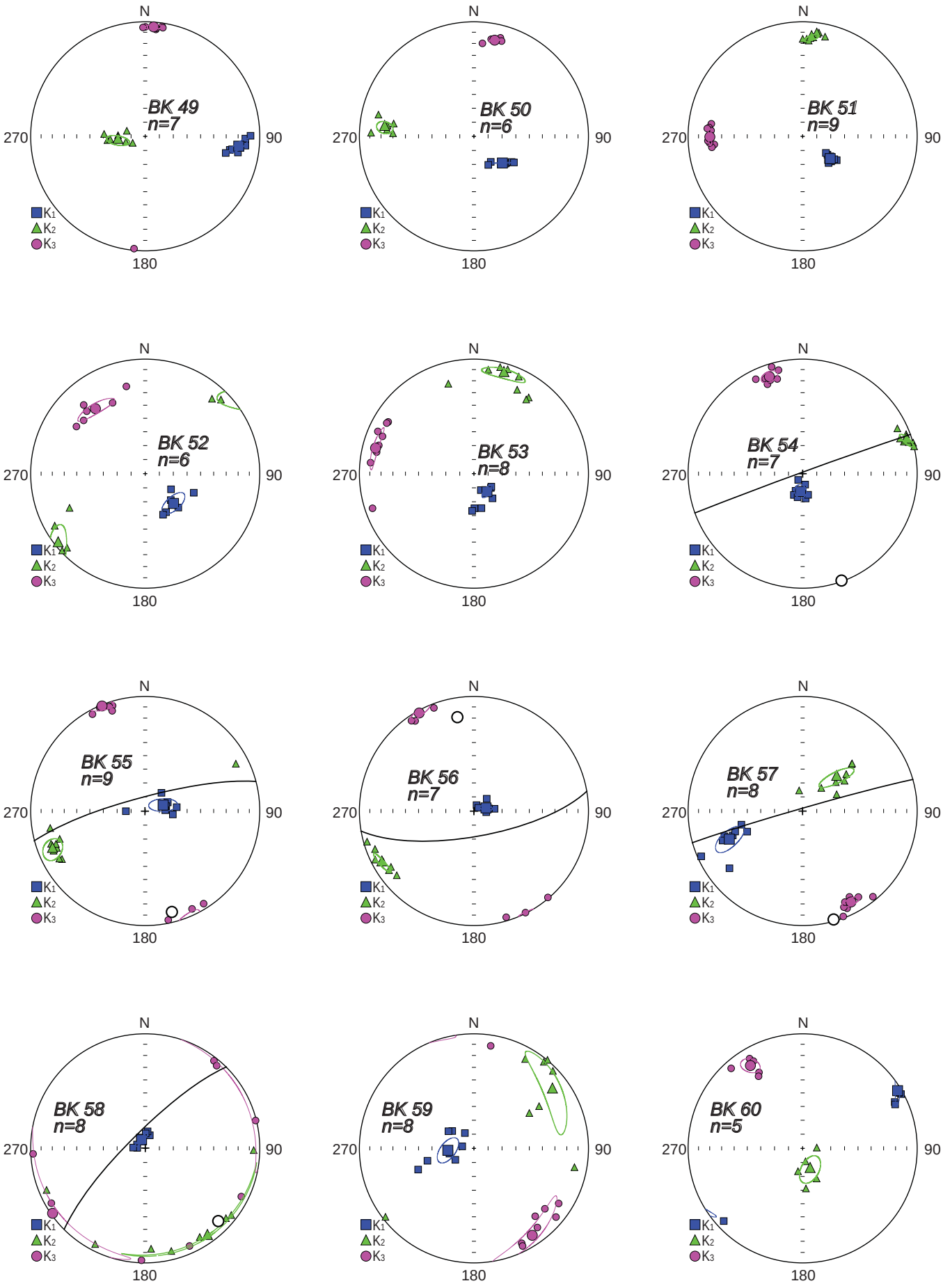

Figure S6 continued

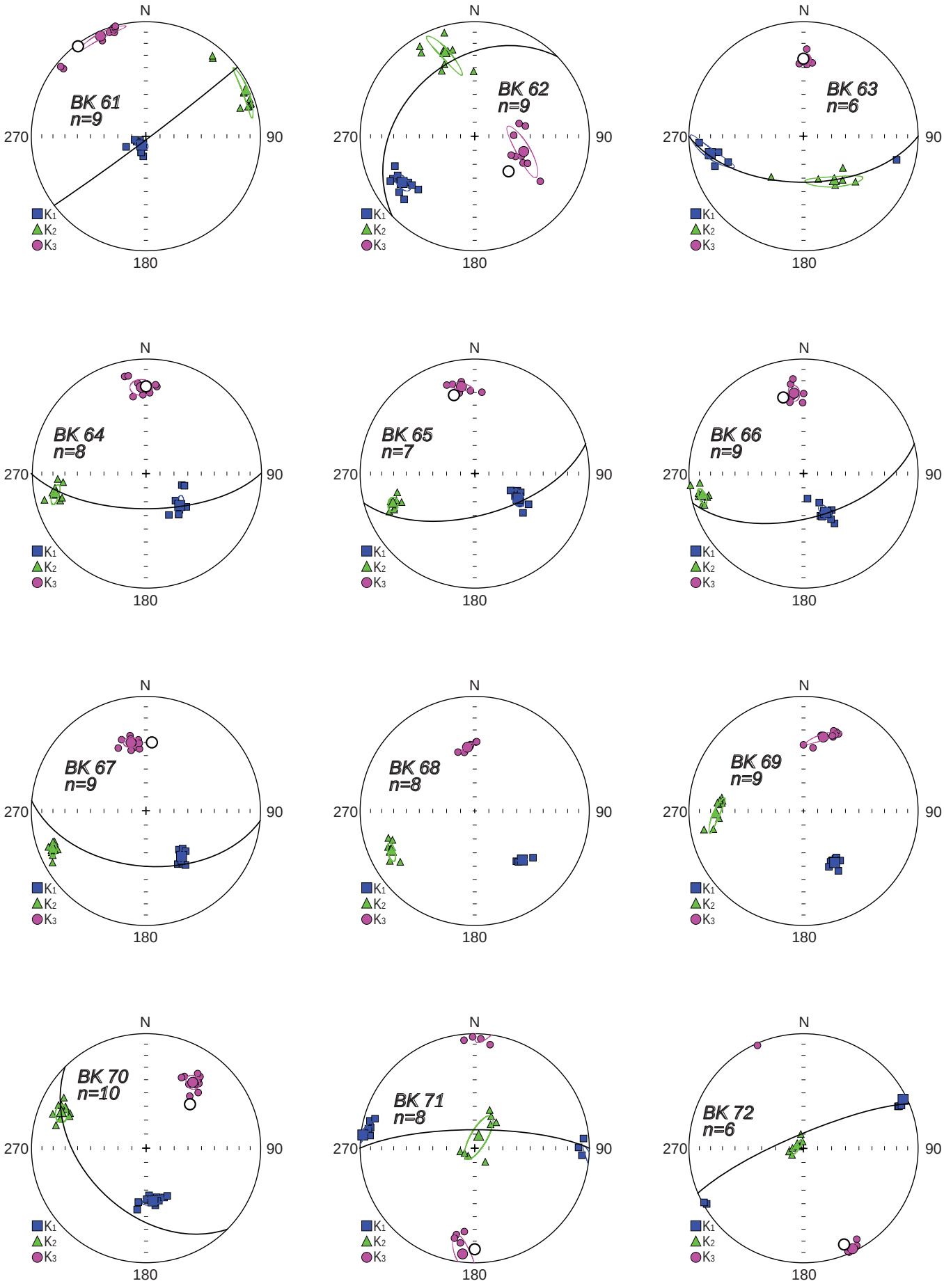

Figure S6 continued

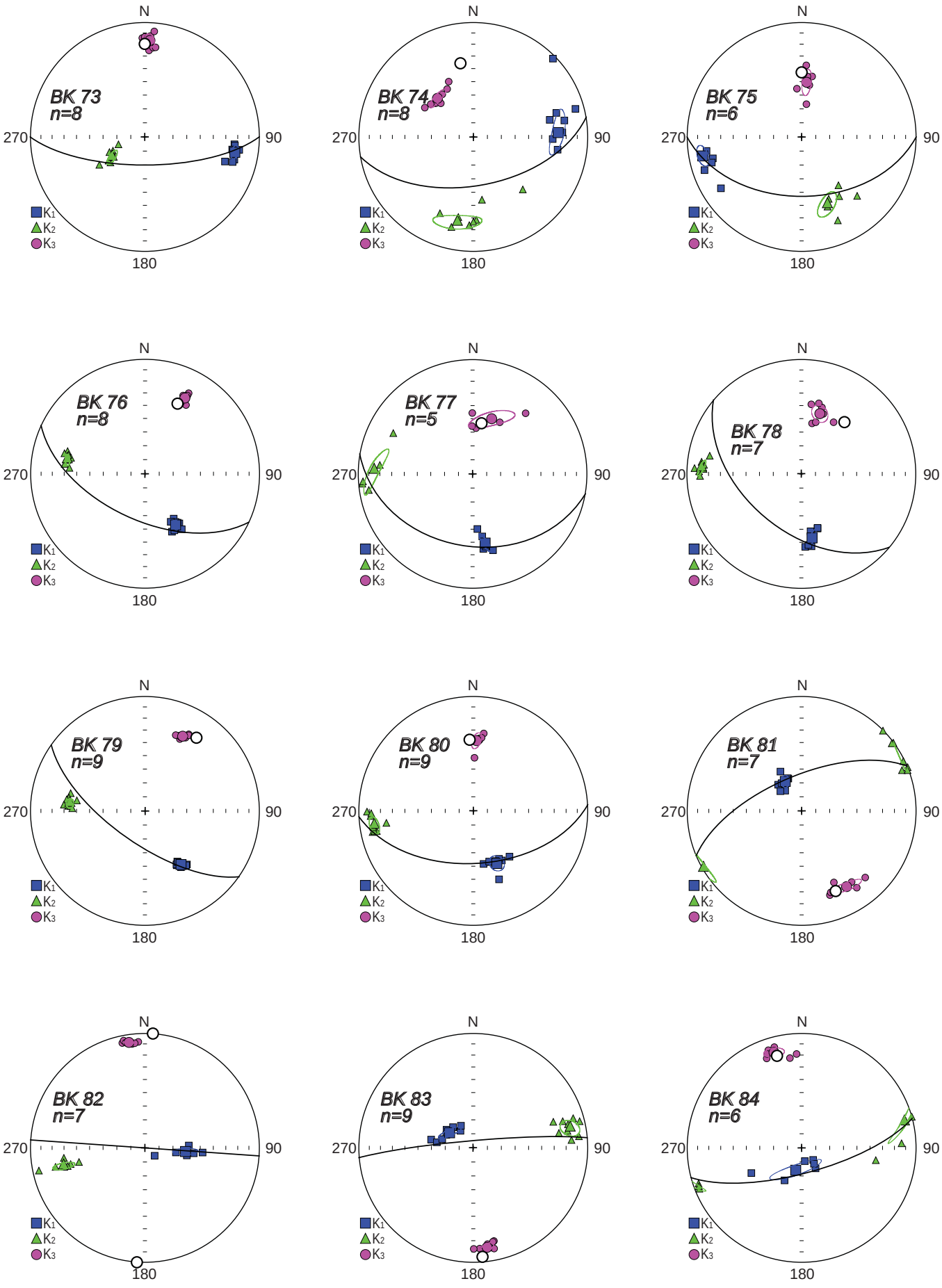

Figure S6 continued

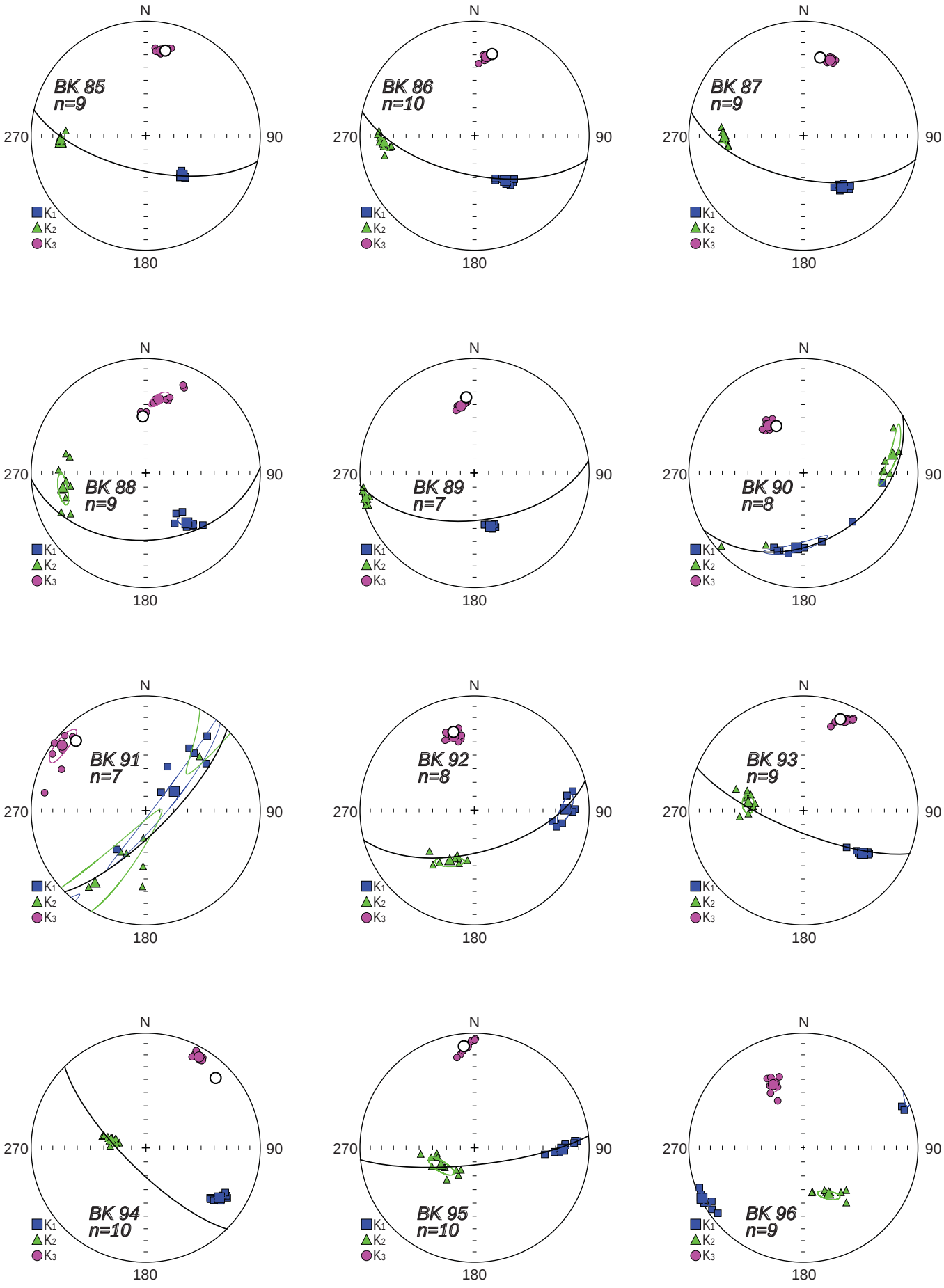

Figure S6 continued